The Journal of Chemical Physics

Modeling and measuring plasmonic excitations in hollow spherical gold nanoparticles

Cite as: J. Chem. Phys. **156**, 094103 (2022); https://doi.org/10.1063/5.0078230
Submitted: 11 November 2021 • Accepted: 07 February 2022 • Accepted Manuscript Online: 07 February 2022 • Published Online: 01 March 2022

Marvin M. Müller, Nanda Perdana, Carsten Rockstuhl, et al.

The Journal of Chemical Physics ARTICLE scitation.org/journal/jcp

Modeling and measuring plasmonic excitations in hollow spherical gold nanoparticles

Cite as: J. Chem. Phys. 156, 094103 (2022); doi: 10.1063/5.0078230
Submitted: 11 November 2021 • Accepted: 7 February 2022 •
Published Online: 1 March 2022

Marvin M. Müller,[1,a] Nanda Perdana,[1] Carsten Rockstuhl,[1,2] and Christof Holzer[1,b]

AFFILIATIONS

[1] Institute of Theoretical Solid State Physics, Karlsruhe Institute of Technology (KIT), 76131 Karlsruhe, Germany
[2] Institute of Nanotechnology, Karlsruhe Institute of Technology (KIT), 76131 Karlsruhe, Germany

Note: This paper is part of the JCP Special Topic on Advances in Modeling Plasmonic Systems.
[a] **Electronic mail:** marvin.mueller@kit.edu
[b] **Author to whom correspondence should be addressed:** christof.holzer@kit.edu

ABSTRACT

We investigate molecular plasmonic excitations sustained in hollow spherical gold nanoparticles using time-dependent density functional theory (TD-DFT). Specifically, we consider Au_{60} spherical, hollow molecules as a toy model for single-shell plasmonic molecules. To quantify the plasmonic character of the excitations obtained from TD-DFT, the energy-based plasmonicity index is generalized to the framework of DFT, validated on simple systems such as the sodium Na_{20} chain and the silver Ag_{20} compound, and subsequently successfully applied to more complex molecules. We also compare the quantum mechanical TD-DFT simulations to those obtained from a classical Mie theory that relies on macroscopic electrodynamics to model the light–matter interaction. This comparison allows us to distinguish those features that can be explained classically from those that require a quantum-mechanical treatment. Finally, a double-shell system obtained by placing a C_{60} buckyball inside the hollow spherical gold particle is further considered. It is found that the double-shell, while increasing the overall plasmonic character of the excitations, leads to significantly lowered absorption cross sections.

I. INTRODUCTION

Plasmonics has become an increasingly important topic that has gathered significant momentum in the past decades.[1–3] More recently, the field of plasmonics has expanded toward quantum technology, focusing on quantum effects that get more important as the size of nanostructures keeps shrinking evermore.[4–7] When quantum effects become relevant, the need for *ab initio* methods to describe these effects immediately emerges. On the verge of this need, methods such as the time-dependent density functional theory (TD-DFT) and corresponding tight-binding (TB) based approaches have become workhorse methods to capture quantum effects observed in plasmonics.[8–15]

Quantum plasmonics, usually involving finite molecules, has become a field on its own, and, therefore, two needs arise. First, there is a need for suitable reference model systems that can be used to evaluate and test certain properties and also to benchmark the performances of different calculation methods. These systems should be small enough for many *ab initio* methods to be applicable to, yet at least to some extent similar and comparable to actual materials that plasmonics is mainly concerned with. Second, a measure for the plasmonic character of an excitation that can be applied fast and robustly after general TD-DFT calculations is desirable to distinguish single-particle molecular transitions from collective plasmonic modes. A method capable of the latter optimally is a simple automatized post-processing tool that evaluates a given mode *a posteriori* at virtually no additional cost if the question arises whether a said mode is mainly of single-particle or plasmonic character. This study aims to meet both needs mentioned above.

Tackling the first point, Mullins *et al.* have recently published their findings of a hypothetical, near-spherical Au_{60} particle that takes the form of a shell and that bears similarity to the famous C_{60} buckyball.[16] The Au_{60} particle has been derived as a subshell of the

dressed Au_{144} particle that has been synthesized and described in the literature.[17–19] This subshell has icosahedral symmetry, belonging to the point group I_h, yet was found to distort toward the I symmetry in the absence of further core shells.[20] Further investigations in Ref. 20 suggest that the charge of the complex has a significant impact on its structure. Adding a single electron or removing one or two electrons from Au_{60}, therefore, yields structures with C_s symmetry only. While the structure and theoretical existence of Au_{60} are interesting on their own from an intellectual perspective, the hollowed-sphere structure of the particle also raises questions concerning the plasmonic character inherited by this exotic species. Molecular plasmons are well-known and investigated in a wide variety of different species.[21–23] However, to link the classical to the quantum world, the special symmetric structure of Au_{60} makes it an ideal candidate to compare classical simulations of spherical homogeneous shells to quantum chemical approaches taking into account the full complexity of the atomic structure. This might be a route to identify the borderline of what classical simulations can achieve in these hollow species.

Tackling the second point, one can expect single-particle-like excitations to mix heavily with plasmonic modes in the Au_{60} molecule. Therefore, it can be looked upon as a perfect test system for the performance of plasmonic classifiers that aim to distinguish both types of resonances. Due to their very nature, classical simulation methods are not sufficiently elaborate to cover both classes of excitations, whereas the quantum mechanical approach is. Therefore, the comparison between classical and quantum mechanical approaches constitutes a further cross-checking mechanism in the identification process to unveil the nature of a given resonance.

As part of the special issue on "Advances in Modeling Plasmonic Systems," this work aims to describe and analyze the features of this near-spherical hollow gold species and characterize the molecular and plasmonic features within their optical spectra at the quantum mechanical level. To account for relativistic effects, we will make use of scalar relativistic TD-DFT,[24–26] which has recently been adapted to be capable of tackling systems of significant size.[27] To identify the appearance of plasmons, we use the recently proposed energy-based plasmonicity index (EPI),[28] which was initially applied within a TB simulation framework, and translate it here for the first time to the TD-DFT language. In contrast to the Coulomb scaling approach,[21] or the generalized plasmonicity index (GPI),[29–31] the EPI has the conceptual advantage of being readily evaluated even for many frequencies or excitation energies. This allows for quick scans of full spectra even if hundreds or thousands of excited states are involved in the optical spectrum of a system. Therefore, an integral part of this study is to demonstrate how the EPI can be calculated using linear-response TD-DFT (LR-TD-DFT) or many-body methods such as the Bethe–Salpeter equation.[64]

Moreover, we compare the optical response of the Au_{60} particle obtained from TD-DFT to predictions that rely on macroscopic electrodynamics in the framework of Mie theory. This allows us to identify those features that emerge already classically qualitatively. Then, we extend the discussion toward the analysis of a multi-shell particle system, in specific, an experimentally feasible double-shell system consisting of a C_{60} inner shell and an Au_{60} outer shell. Interestingly enough, while increasing the overall plasmonic character of the excitations, the double-shell system exhibits a significantly lowered absorption cross section, both in the classical and the quantum mechanical calculations.

II. METHODS

In this section, we describe the methods used to model the plasmonic systems of interest. First, we outline how the classical homogeneous shells are modeled in the context of macroscopic Maxwell's equations. Material properties are taken into account based on a dielectric function. Admittedly, such treatment is on the edge of what is acceptable for the structures considered. Still, as we will notice, on a qualitative level, selected properties that we obtain quantum-mechanically are reproduced by such a classical approach rather accurately. Afterward, we describe the framework of our quantum chemical simulations. For completeness, we also shortly outline selected approaches previously applied to judge the character of an excitation and explain in detail the application of the EPI in the TD-DFT framework. In Sec. III, these methods are used to study the plasmonic systems of interest.

A. Mie theory and T-matrix approach

Mie theory constitutes the most widely used theoretical tool to describe the electromagnetic scattering of light by a spherical particle analytically.[32,33] In this approach, to take into account the symmetry of the problem, the incident field $\mathbf{E}_{\mathrm{inc}}(\mathbf{r})$ and scattered field $\mathbf{E}_{\mathrm{sca}}(\mathbf{r})$ induced by the sphere oscillating at a fixed frequency ω are expanded into a series of vector spherical harmonic functions (VSHF) $\mathbf{M}_{mn}^{(J)}(\mathbf{r})$ and $\mathbf{N}_{mn}^{(J)}(\mathbf{r})$,

$$\mathbf{E}_{\mathrm{inc}}(\mathbf{r}) = \sum_{n=1}^{\infty}\sum_{m=-n}^{n} p_{mn}\mathbf{N}_{mn}^{(1)}(\mathbf{r}) + q_{mn}\mathbf{M}_{mn}^{(1)}(\mathbf{r}), \tag{1}$$

$$\mathbf{E}_{\mathrm{sca}}(\mathbf{r}) = \sum_{n=1}^{\infty}\sum_{m=-n}^{n} a_{mn}\mathbf{N}_{mn}^{(3)}(\mathbf{r}) + b_{mn}\mathbf{M}_{mn}^{(3)}(\mathbf{r}). \tag{2}$$

Here, p_{mn}, q_{mn} and a_{mn}, b_{mn} are the expansion coefficients of the incident and scattered fields, respectively. To study the details of the light–matter interaction, these coefficients can be related by introducing the corresponding T-matrix T of the scattering object,[34]

$$\begin{pmatrix} a_{11} \\ \vdots \\ a_{mn} \\ b_{11} \\ \vdots \\ b_{mn} \end{pmatrix} = T \begin{pmatrix} p_{11} \\ \vdots \\ p_{mn} \\ q_{11} \\ \vdots \\ q_{mn} \end{pmatrix}. \tag{3}$$

The T-matrix can be obtained numerically for complicated objects, but analytical solutions can be used for the spherical objects considered here.[35] Under the assumption of linearly polarized plane wave illumination, the obtained T-matrix contains information on many

measurable quantities in the far-field. For our purpose, the quantities of interest are the scattering cross section $C_{\mathrm{sca}}(\omega)$, extinction cross section $C_{\mathrm{ext}}(\omega)$, and absorption cross section $C_{\mathrm{abs}}(\omega)$, which are computed according to Ref. 36,

$$C_{\mathrm{sca}}(\omega) = \frac{2\pi}{k^2}\,\mathrm{Tr}(|T|^2), \tag{4}$$

$$C_{\mathrm{ext}}(\omega) = -\frac{2\pi}{k^2}\mathrm{Re}[\mathrm{Tr}(T)], \tag{5}$$

$$C_{\mathrm{abs}}(\omega) = C_{\mathrm{ext}}(\omega) - C_{\mathrm{sca}}(\omega), \tag{6}$$

where $k = \frac{\omega}{c}\sqrt{\varepsilon_{\mathrm{background}}(\omega)}$ corresponds to the wavenumber in the background medium characterized by an isotropic permittivity $\varepsilon_{\mathrm{Background}}(\omega)$. The numerical calculations involved in this approach have been conducted with MATLAB.[37]

B. Time-dependent density functional theory

It is well-known that plasmonic excitations arise in standard quantum mechanical calculations, e.g., in the widely used TD-DFT ansatz. Within TD-DFT, the excitation energies are obtained from the solutions of a generic eigenvalue problem,[38–40]

$$\begin{pmatrix} A & B \\ B^* & A^* \end{pmatrix}\begin{pmatrix} X \\ Y \end{pmatrix} = \omega\begin{pmatrix} 1 & 0 \\ 0 & -1 \end{pmatrix}\begin{pmatrix} X \\ Y \end{pmatrix}. \tag{7}$$

The orbital rotation matrices A and B are defined as

$$A_{ia,jb} = (\varepsilon_i - \varepsilon_a)\delta_{ij}\delta_{ab} + (ai|jb) + f^{\mathrm{XC}}_{ai,bj}, \tag{8}$$

$$B_{ia,jb} = (ai|bj) + f^{\mathrm{XC}}_{ai,bj}, \tag{9}$$

where ε_i is the energy of the ith Kohn–Sham eigenstate ϕ_i, $(ai|bj)$ is a Coulomb integral,

$$(ai|bj) = \int \phi_a(r)\phi_i(r)\frac{1}{|r-r'|}\phi_b(r')\phi_j(r')\mathrm{d}r\mathrm{d}r', \tag{10}$$

and

$$f^{\mathrm{XC}}_{ai,bj} = \frac{\partial^2 E^{\mathrm{XC}}}{\partial D_{ai}\partial D_{bj}} \tag{11}$$

is the exchange–correlation kernel of the density functional approximation within the adiabatic approximation. Properties such as oscillator strengths, excited-state dipole moments, or nuclear forces, for instance, can be obtained straightforwardly from the solutions of the eigenvalue problem of LR-TD-DFT.[41]

C. Resonance classifiers

While there is no strict differentiation within quantum mechanics between single-particle excitations and plasmonic modes, one is often interested in characterizing excitations from a conceptional point of view. Various indicators have been suggested in the literature to distinguish single-particle excitations from plasmonic modes in molecular simulations. A selection of these techniques will be shortly introduced and discussed at this point. We will also explain why we specifically rely here on the EPI as a classifier and outline how to obtain it from the outcome of TD-DFT simulations.

1. Coulomb scaling approach

The ansatz from Bernadotte *et al.* exploits the shifting behavior of the energy of plasmonic peaks under the scaling of the electronic interaction parts of the eigenvalue problem, which include both the Coulomb integral and the exchange–correlation kernel.[21] While single-particle-like excitations are found to remain spectrally stable, plasmonic peaks exhibit a blue shift when the interaction scaling parameter λ is increased. The orbital rotation matrices A and B in this framework read

$$A_{ia,jb} = (\varepsilon_i - \varepsilon_a)\delta_{ij}\delta_{ab} + \lambda\left[(ai|jb) + f^{\mathrm{XC}}_{ai,bj}\right], \tag{12}$$

$$B_{ia,jb} = \lambda\left[(ai|bj) + f^{\mathrm{XC}}_{ai,bj}\right]. \tag{13}$$

As λ in Eqs. (12) and (13) is varied from 0 to 1, plasmons exhibit a behavior different from molecular excitations, being quenched at $\lambda = 0$ and moving significantly to the blue with their excitation energy when going to $\lambda = 1$. While this is conceptually easy to access, it requires the performance of a series of TD-DFT calculations, each with a slightly different prefactor λ for the electronic interaction part. In this process, energy level crossings often occur, and, therefore, a graphical analysis (root-following) needs to be done to identify plasmonic excitations reliably. Especially for larger systems with a high density of states, the generation of points with different values of λ may, however, become extremely costly, which is a clear disadvantage. In addition, root-following may be error-prone in this high-density regime.

2. Generalized plasmonicity index (GPI)

The GPI[29–31] of a classical system is defined as the ratio of the induced energy and external energy of a system's response at frequency ω,

$$\eta(\omega) = \frac{\left|\int \mathrm{d}^3\mathbf{r}\,\rho_c^{\mathrm{ind}}(\mathbf{r},\omega)v^*_{\mathrm{ind}}(\mathbf{r},\omega)\right|}{\left|\int \mathrm{d}^3\mathbf{r}\,\rho_c^{\mathrm{ind}}(\mathbf{r},\omega)v^*_{\mathrm{ext}}(\mathbf{r},\omega)\right|}, \tag{14}$$

where v_{ind} and v_{ext} are the induced potential and the applied external potential, respectively. Moreover, ρ_c^{ind} denotes the classical real-space induced charge density and "*" means complex conjugation.

In quantum mechanical systems investigated by TD-DFT, the GPI of an excited state ζ can be computed based on the Coulomb energy of its real-space induced density and the inverse of its decay rate Γ_ζ,

$$\eta_\zeta = \frac{1}{\Gamma_\zeta}\int \frac{\rho^*_\zeta(\mathbf{r})\rho_\zeta(\mathbf{r}')}{|\mathbf{r}-\mathbf{r}'|}\mathrm{d}^3\mathbf{r}\mathrm{d}^3\mathbf{r}'. \tag{15}$$

The excited state density $\rho_\zeta(r)$ is generally accessible from the solutions of Eq. (7) as

$$\rho_\zeta(\mathbf{r}) = \sum_{ia}\left[X_{ia,\zeta}\phi_i^\dagger(\mathbf{r})\phi_a(\mathbf{r}) + Y_{ia,\zeta}\phi_a^\dagger(\mathbf{r})\phi_i(\mathbf{r})\right]. \tag{16}$$

Unlike in the Coulomb scaling approach outlined in Subsection II C 1, only a single post-processing step is needed to compute the GPI. In that sense, the GPI is superior from an ease-of-use point of view, yet still, it induces a significant post-processing overhead, especially in a situation with a high density of states. Moreover, the GPI is not normalized to a given interval. Consequently, to interpret the obtained numbers, the entire spectrum of the GPI for a given structure or at least a sufficiently high number of peaks needs to be investigated. Like the Coulomb scaling approach, the GPI can also detect and classify dark plasmons,[42–45] where the latter have been observed for interacting nanoparticles.[45] In general, the scaling approach and the GPI provide consistent classification results, as both methods rely on the induced charge and the resulting induced potential and interaction energy.

3. Sloshing and inversion population dynamics

Townsend and Bryant[46–48] propose to analyze the temporal evolution of the electronic population of Kohn–Sham single-particle eigenstates in real-time TD-DFT. To that end, they illuminate gold jellium spheres with monochromatic light at different resonant frequencies and find two qualitatively different dynamical behaviors. For a first set of modes, the contributing single-particle states are continuously occupied by electrons or depleted in a monotonous *inversion* manner. These modes are classified single-particle-like, featuring induced charges in real space, mostly in the sphere's core. In contrast, for a second set of modes, the involved states gain or lose population in a more complex *sloshing* manner. The charge is shifted from states just below the Fermi level to states just above and back again in an oscillatory way. The associated modes are classified plasmonic, exhibiting induced charge mostly at the surface of the spheres—reminiscent of a classical plasmonic charge cloud oscillation. The EPI introduced below quantitatively measures the extent of inversion type and sloshing type contributions to the formation of a given mode.

This approach is conceptually different from the previous two as it targets the quantum mechanical origin of the mode in energy space rather than its real-space embodiment. The classification results, therefore, are not always consistent. It has been shown, for instance, that the strong dipolar longitudinal response in polyacene molecules[49] and linear polyene chains[50] intrinsically belongs to the HOMO–LUMO transition of said systems. The real-space-based GPI and the scaling approach clearly classify these modes as plasmonic, whereas Townsend and Bryant and the EPI might conclude that they are single-particle-like, having in mind their single-particle-like energy-space origin.

4. Energy-based plasmonicity index (EPI)

Recently, another ansatz based on the electronic interaction energy in a quantum mechanical system, the EPI, has been proposed[28] and applied in a detailed analysis within a tight-binding framework.[51] In this work, we show that the EPI can be successfully applied to DFT-based simulation schemes and outline how it is calculated using LR-TD-DFT. Like the GPI, the EPI is expressed in terms of the transition density of an excitation ζ. However, unlike in the case of the GPI, the real-space induced density is not the quantity that predominantly determines the EPI, but coherence dynamics, i.e., off-diagonal elements in the density that couple different energetic states, need to be taken into account. To obtain the EPI, starting from the transition density in the Kohn–Sham molecular orbital basis,

$$\rho_{ai}^\zeta = \left[X_{ia,\zeta} + Y_{ia,\zeta}\right], \tag{17}$$

a modified transition density $\tilde{\rho}^\zeta$ is used,

$$\tilde{\rho}_{ai}^\zeta = \frac{|\rho_{ai}^\zeta|}{\|\varepsilon_a - \varepsilon_i| - \omega_\zeta + \mathrm{i}\eta|^2}, \tag{18}$$

that amplifies ρ^ζ as $|\varepsilon_a - \varepsilon_i|$ approaches ω_ζ. $\mathrm{i}\eta$ serves as a regularization parameter preventing numerical overflows. The EPI is then calculated from a similarity measure of $\tilde{\rho}^\zeta$ and ρ^ζ in either the atomic orbital (AO) or the molecular orbital (MO) basis,

$$\mathrm{EPI}^{\mathrm{MO}}(\omega_\zeta) = 1 - \langle\tilde{\rho}_{ai}^\zeta, \rho_{ai}^\zeta\rangle \in [0,1], \tag{19}$$

$$\mathrm{EPI}^{\mathrm{AO}}(\omega_\zeta) = 1 - \langle\tilde{\rho}_{\mu\nu}^\zeta, \rho_{\mu\nu}^\zeta\rangle \in [0,1], \tag{20}$$

where the scalar product $\langle a, b\rangle$ is given by Eq. (8) of Ref. 28. Furthermore, $\rho_{\mu\nu}$ is obtained from the energy-weighted excited state density and the Kohn–Sham orbital coefficient C as

$$\rho_{\mu\nu} = \sum_{ai} C_a^\mu C_i^{\nu*}\rho_{ai}. \tag{21}$$

The EPI in the AO and MO basis differ by the overlap matrix, which is contained in the AO variant through the Kohn–Sham orbital coefficients. Plasmonic resonances are foremost determined by electronic interaction energy. Hence, they will induce smaller differences in $\tilde{\rho}^\zeta(\mathbf{r})$ with respect to $\rho^\zeta(\mathbf{r})$, since the excitation energy ω_ζ does, in general, not match the transition energy $|\varepsilon_a - \varepsilon_i|$, as it is expected for single-particle-like resonances. As a result, plasmonic resonances yield higher EPI values than single-particle-like excitations. The EPI is sensitive to dark plasmons and normalized to the interval $[0,1]$. Moreover, it is very suitable for fast post-processing even if many excitations or frequencies have to be analyzed. We note that by plugging the definition of the excited state density Eq. (16) into Eq. (18), the EPI is calculated in energy space rather than in real space, which is the case for the GPI. It should be noted that the absolute values of the EPI of a given mode in a given structure may not coincide when computed with different simulation methods. However, it always holds that higher EPIs reflect a stronger plasmonic behavior. We generally find lower EPIs in TD-DFT simulations as compared to TB-based methods, where the underlying basis set is eventually much smaller. Therefore, it is not possible to give a threshold value above which an excitation should be

considered plasmonic. To directly compare the EPIs of the most prominent modes in different structures, one should ensure that the simulation method is the same in all the cases and the underlying basis set of comparable size.

D. Computational details

As initial test cases, to validate and verify the EPI implementation, we calculate the corresponding spectra and EPIs for the well-investigated linear Na_{20} chain,[21] as well as for the tetrahedral Ag_{20} structure.[21,52] Furthermore, as outlined in the Introduction, the actual species of interest is the charge-neutral Au_{60} molecule with I symmetry. To test the structural and charge effects on the plasmonic and single-particle excitations, we performed DFT and TD-DFT calculations on the closed-shell I_h symmetric Au_{60}^{4+} and Au_{60}^{6-} species.

The Ag_{20} geometry was taken from Ref. 53. For Na_{20}, a linear chain with Na–Na distances of 2.89 Å was assumed, as described in Ref. 54. Geometries for the Au_{60} clusters were optimized using the TPSS functional[55] in conjunction with the dhf-TZVPP basis set.[56] The D4 dispersion correction was used during geometry optimization.[57] For absorption spectra of the metallic Na_{20}, Ag_{20}, and the Au_{60} systems, the TPSS functional[55] was used together with the dhf-TZVPP basis set.[56] Scalar-relativistic absorption spectra were calculated using standard LR-TD-DFT. Furthermore, out of theoretical interest, we also investigated the double-shell system C_{60}@Au_{60}, where a C_{60} fullerene is embedded into the Au_{60} shell. For C_{60}@Au_{60}, geometries are optimized using the TPSS and the dhf-split-valence-polarization (SVP) basis set. The absorption spectra were then calculated by the modified PSTS (mPSTS) local hybrid functional (LHF).[58,59] LHFs employ a position-dependent admixture of exchange energy, yielding superior results for molecular single-particle excitations.[59] For all excitations, the EPI is calculated using, as outlined, Eqs. (18) and (19). The procedure has been implemented in a locally modified version of TURBOMOLE 7.6.[60] and will be publicly released in the next version. All LHF calculations employed the seminumerical semiJK algorithm.[27] For all TPSS calculations, a grid of size 4 was used, while for the mPSTS LHF, we employed a "veryfine" grid.[27] All evaluated excitation energies, oscillator strengths, and corresponding EPI values used to generate the graphics in Sec. III can be found in the supplementary material.

In the classical calculations, we employ a homogeneous and isotropic spherical gold shell nanoparticle with a shell thickness equal to the empirical diameter of the gold atom (d_{Au} = 0.27 nm)[61] and its radius equal to the radius of the Au_{60} compound (r_{Au} = 0.60 nm). These parameters have been derived from the optimized geometry in the quantum mechanical *ab initio* simulations. For the multi-shell system, we model the C_{60} buckyball by a carbon shell using effective material parameters of one-atom-thick extended graphene.[62] The carbon shell thickness is approximated by the empirical diameter of the carbon atom (d_C = 0.14 nm), and its radius (r_C = 0.395 nm) adapted such that no void is left between both shells.

III. RESULTS AND DISCUSSION

At first, we investigate the linear Na_{20} and tetrahedral Ag_{20} systems, which are used as test cases for the EPI as they feature well-known plasmonic excitations. Afterward, the recently described Au_{60} buckyball is investigated. The latter is an interesting species for describing plasmonic effects.[16] In this section, we first discuss the neutral species and two charged configurations of it. After that, we put emphasis on the C–Au double-shell system.

A. EPI in the linear Na_{20} chain

The sodium chain was used by Bernadotte *et al.* to validate the Coulomb scaling approach described in Ref. 21. Within the irreducible representation Σ_u^+, two peaks are observed in the absorption spectrum in the energy range from 0 to 2 eV, both originating from plasmonic excitations. Although further modes exist, those exhibit considerably lower oscillator strengths and are not identified as plasmons.

Figure 1 shows the absorption spectrum of the Na_{20} chain alongside the corresponding EPI values calculated both in the AO and MO basis. Both clearly indicate the strong plasmonic character of the two peaks, in excellent agreement with the Coulomb scaling approach.[21] Remaining, less intense excited states exhibit distinctly lower EPI values, especially within the MO basis representation in Fig. 1(a). Applying the GPI to the linear Na_{20} chain also identifies two very strong plasmons, in good agreement with the Coulomb scaling approach.[29] Additionally, peaks with reduced but significant plasmonic character are also hinted at from the GPI, e.g., at around 1.3 eV[29] with roughly 1/4 of the GPI value obtained for the main peaks. This is in excellent agreement with the EPI in the AO basis, exhibiting a very similar behavior; see Fig. 1(b). Given the significantly reduced effort of performing an EPI analysis compared to the Coulomb scaling and GPI approaches, these results are very promising.

B. EPI in the tetrahedral Ag_{20} cluster

The tetrahedral Ag_{20} cluster exhibits a more complicated electronic structure. The Coulomb scaling approach hints at three plasmonic excitations, two of them being dark. The main peak again exhibits a plasmonic character but crosses paths with a single-particle excitation at a Coulomb scaling parameter near 1.

In Fig. 2, we present the absorption spectrum alongside the EPI of the Ag_{20} compound. The EPI can correctly classify the three plasmonic excitations in the presented energy range, which exhibit distinctly higher EPI values than the single-particle ones. The EPIs in the AO representation are slightly more pronounced this time, reaching a value of 0.16 for the main peak, compared to 0.11 in the MO basis. Using the GPI, the small shoulder of the main peak is also identified as plasmonic excitation.[29] This is explained by the mixing of the two different excitations close to full coupling strength. To verify this behavior, we repeated the EPI calculation using the PBE functional, which was used in Ref. 29, but obtained virtually the same EPI values. For this mode, the EPI and GPI differ for the reasons outlined in the last paragraph of Sec. II C 3.

From this validation analysis, it can be concluded that the classification results of the EPI generally coincide with the Coulomb scaling and the GPI approaches unless for very contrived exemptions. An example thereof is the HOMO–LUMO transition in a linear polyene chain, which also exhibits a significant dipole moment

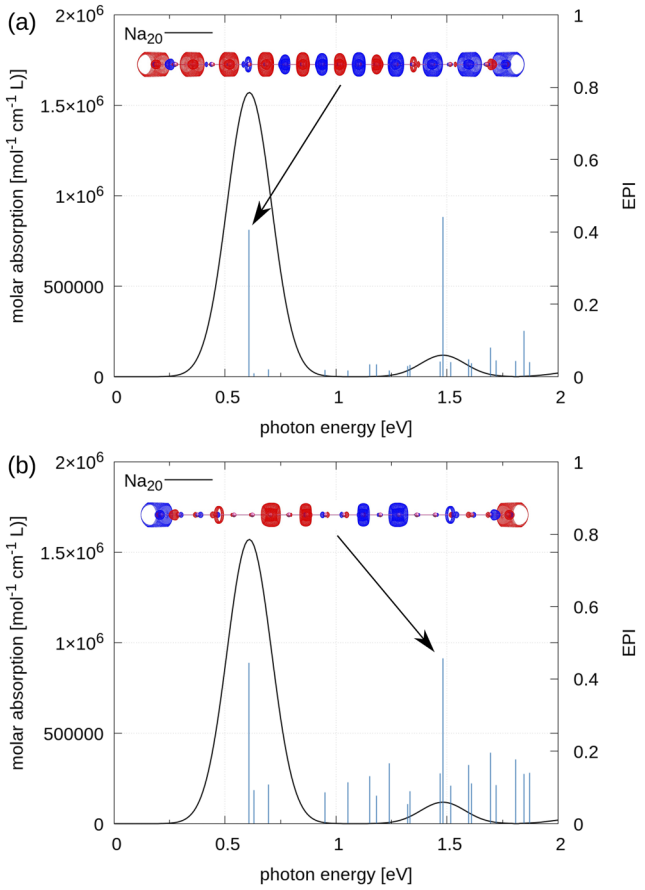

FIG. 1. Absorption spectrum of the Na_{20} linear chain obtained from TPSS/dhf-TZVPP (black solid line). An arbitrary Gaussian broadening of 0.10 eV has been applied. Blue stick spectra indicate the EPI values in (a) MO basis and (b) AO basis and are independent of the molar absorption coefficient. The inset in (a) is the transition density of the plasmonic excitation at 0.6. The inset in (b) is the transition density of the plasmonic excitation at 1.5 eV. An isovalue of 0.0005 a.u. has been used.

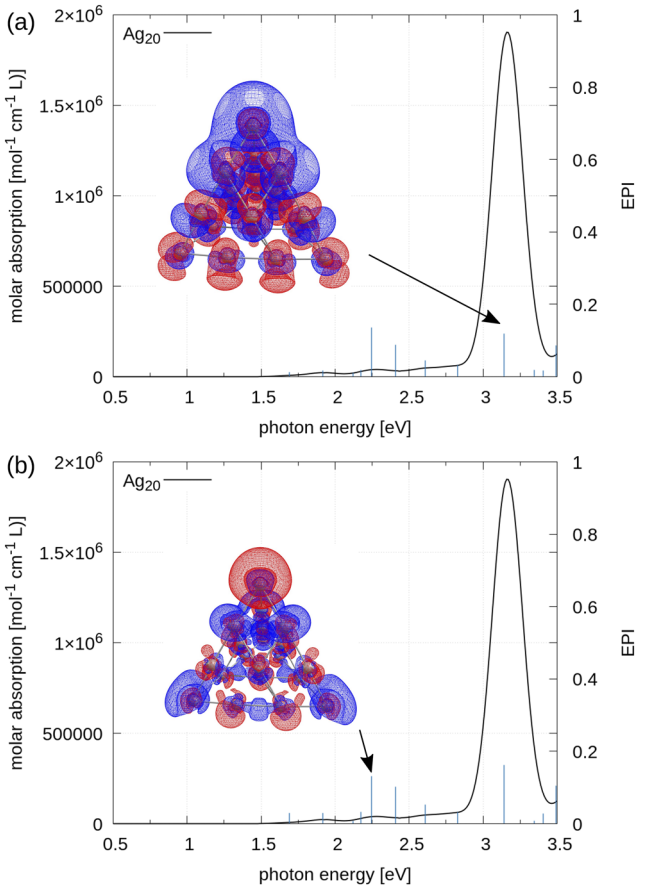

FIG. 2. Absorption spectrum of the tetrahedral Ag_{20} cluster obtained from TPSS/dhf-TZVPP (black solid line). An arbitrary Gaussian broadening of 0.10 eV has been applied. Blue stick spectra indicate the EPI values in (a) MO basis and (b) AO basis and are independent of the molar absorption coefficient. Insets are the transition densities of the two most prominent plasmonic excitations, marked with arrows. An isovalue of 0.0005 a.u. has been used.

in real space—even in the absence of Coulomb interaction.[50] Therefore, the GPI classifies the mode as plasmonic, whereas the EPI does not. As the latter is considerably cheaper to evaluate than any of the other, it can be applied to analyze molecular systems quickly and reliably. In Secs. III and III D, the EPI in the MO basis will be used, as it exhibits a similar behavior to the GPI for the Na_{20} chain and exhibits a more pronounced plasmonic character for the main peak in the Ag_{20} cluster.

C. Optical spectra of the Au_{60} shell with different charges

First, we investigate the optical absorption spectra for the Au_{60} molecule in differently charged and neutral states. Unlike the authors of Ref. 20, who focused on the electronic and geometric structures of the (lower symmetry) anionic and dicationic systems, we are interested in the neutral system as well as those charged states restore the highly symmetric icosahedral I_h symmetry common to other "buckyball" systems. Therefore, three possible charge states are of particular interest. First, the neutral one, belonging to the spatial point group I. Second, a 4+ charged cation, and third, a 6− charged anion. The latter two belong to the highly symmetric icosahedral point group I_h. The simulated optical spectra of these three species and the corresponding EPI values of the excitations, shown as stick spectra of the corresponding color, are depicted in Fig. 3.

The spectrum of the neutral Au_{60} (purple dashed line) yields three absorption peaks in the range between 0.5 and 3.5 eV. A set of relatively high EPI values is located in the band at ~2.2 eV, where the excitations contribute to the lowest-energy peak. Therefore, we conclude that this mode has the most pronounced plasmonic character in this spectrum and probably marks the onset of the typical gold plasmon in that spectral region.

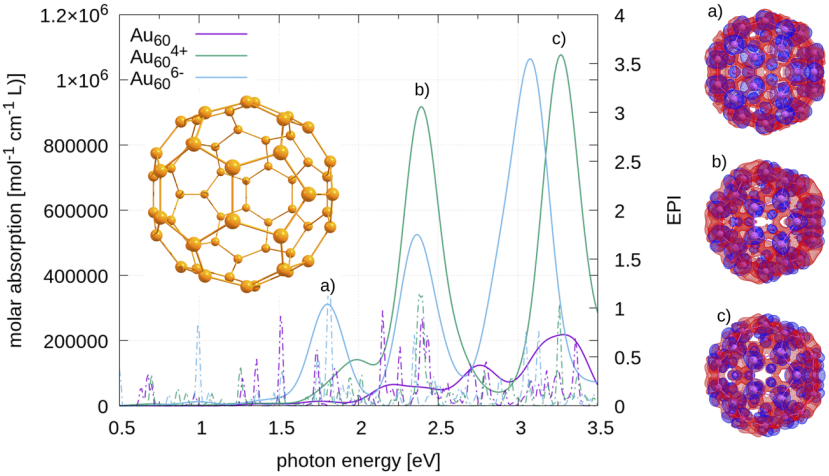

FIG. 3. Absorption spectra of Au_{60} (I), Au_{60}^{4+}, and Au_{60}^{6-} (I_h) obtained from TD-TPSS/dhf-TZVPP. An arbitrary Gaussian broadening of 0.10 eV has been applied to the optical spectra. Dashed–dotted lines indicate corresponding EPI spectra, which have been broadened by 0.01 eV. (a) Peak at ~ 1.8 eV, right: transition density generated for this peak. (b) Peak at ~ 2.4 eV, right: transition density generated for this peak. (c) Peak at ~ 3.3 eV, right: transition density generated for this peak. Transition densities have been generated from Au_{60}^{4+}. Red indicates a gain in electron density and blue indicates a loss in electron density. An isovalue of 0.0005 a.u. has been used.

Figure 4(a) shows the spectrum of a spherical homogeneous hollow gold shell (blue line) with a diameter of 0.6 nm and a thickness of 0.27 nm obtained by the classical Mie theory. Moreover, we present the absorption cross section of the same structure for varying shell thicknesses in Fig. 4(b). If the thickness of the shell is decreased, such that it resembles more closely the considered hollow gold shell, one can observe that the plasmonic absorption peak tends to redshift, and its amplitude gets enhanced. Only for an extremely thin shell thickness, the strength of the absorption cross section decreases in the plasmonic resonance as the available volume of polarizable matter decreases. On the other hand, if the thickness of the shell increases, we adiabatically approach the spectra of a bulk sphere. As a result, the spectral position of the resonance is rather blue-shifted into a spectral region where gold tends to be absorptive. This lowers the resonance strength and broadens it. The red dashed line marks the shell thickness $d_{\mathrm{Au}} = 0.27$ nm used in our classical simulations. This value is taken from the empirical diameter of the gold atom. However, as shown in Fig. 4(b), the absorption cross section is relatively insensitive to the shell thickness in the region of interest, such that this choice is not crucial for the results of our simulations. As we cannot assume to capture the full atomistic inter-band single-particle transition dynamics of the molecule within our classical macroscopic approach, we attribute the prominent resonance around 2.4 eV to the classical plasmon resonance of the shell. Conversely, we deem the higher-energy prominent modes in the TD-DFT spectrum above 2.5 eV of predominantly single-particle origin. There are exceptions to this, as, e.g., a single prominent plasmonic mode at 3.25 eV for the Au_{60}^{4+} buckyball, depicted in Fig. 3. However, the density of high-EPI excitations in this region of the spectrum is low compared to the region around 2.4 eV. In contrast to the simpler examples outlined in the previous sections, for enlarged systems, it is, therefore, more subtle to classify absorption bands as plasmonic or single-particle-like, when, indeed, they are combinations of both. Therefore, it may be beneficial to investigate the accumulated EPI, similar to broadened spectra, for more complex molecular structures. Nevertheless, we, indeed, find a surprisingly accurate correspondence for the neutral species between classical and *ab initio* TD-DFT results, both unveiling a plasmonic mode in the range between 2.1 and 2.5 eV.

The two charged cationic and anionic (icosahedral) $Au_{60}^{(4+,6-)}$ molecules generally exhibit much stronger resonances in Fig. 3 as compared to the neutral species. The Au_{60}^{6-} anion (blue line) has three pronounced peaks in the shown region, whereas the cation's lowest-energy mode is merging into the shoulder of the much stronger mode around 2.3–2.4 eV (green line). In both cases, this mode at 2.3–2.4 eV, where the classical gold plasmon resides, possesses a significantly enhanced plasmonic character, perceptible through the high density of high EPI values in this window for many contributing excitations. Furthermore, the bands below 2.0 eV of the anionic gold buckyball exhibit strong plasmonic character, with EPIs exceeding values of 0.2. The latter peak is also significantly more pronounced for the anionic species than for the other two molecules. However, compared to the cation, the band at 2.4 eV is significantly less pronounced. Analysis of the transition densities of the most relevant excitations, marked with (a)–(c) and shown in the right of the figure, reveals that these excitations are strongly delocalized across the entire molecule. In all three cases, the electron density is depleted from the vicinity of the nuclei and pumped toward the bonding regions. The lower the excitation energy, the more delocalized this overall distribution is, as indicated by the reduction in "white spaces" when going from (c) to (a) in Fig. 3. Analyzing the depicted transition densities together with the EPI strongly suggests that the icosahedral gold buckyballs are well suited as convenient toy systems when modeling quantum plasmonics. Both molecules, anionic and cationic species, exhibit intense peaks near the actual gold plasmon. The fact that the icosahedral Au_{60} moiety is observed in larger Au_{144} nanoparticles as well further suggests that this is a hypothetical yet also a practical model for this task.

While still viable as preliminary test molecules, the highly symmetric charged particles are likely better candidates for modeling and studying quantum plasmonics than the neutral one. If an actual pathway for the synthesis of the Au_{60} moiety is discovered, the charged species should also be studied in detail as they may offer superior (optical) properties in some respects.

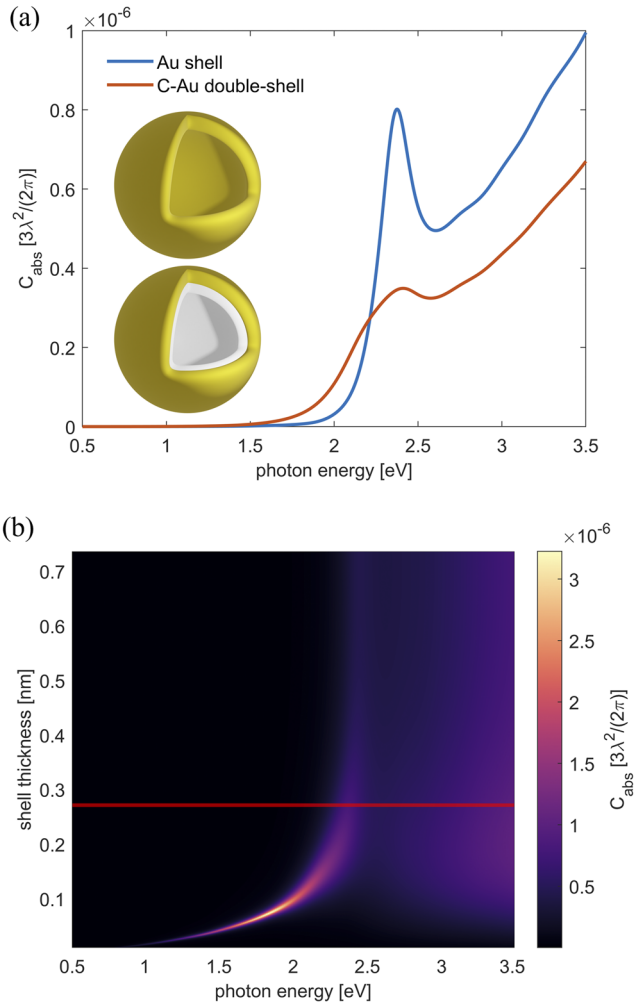

FIG. 4. (a) Absorption cross section of a gold nanoshell and a carbon–gold double-shell system, which mimics the C_{60}@Au_{60} compound, calculated with the T-matrix approach. (b) Absorption cross section of a gold shell with varying shell thickness. The red line represents the calculated double-shell system configuration (d_{Au} = 0.27 nm).

D. Plasmons in a C_{60}@Au_{60} double-shell system

With the ability to inscribe a C_{60} fullerene buckyball into the Au_{60} molecule in a stable way, Ref. 16 provides another interesting pathway one could take in expanding the knowledge about plasmons in highly symmetric hollow molecules.

Figure 4(a) shows the absorption cross section of the C–Au double-shell structure (red line) obtained from the classical Mie theory. It exhibits a relatively broad absorption maximum at ~2.4 eV. However, compared to the gold single-shell, the mode is much less distinct, and less than half the amplitude as the carbon shell is inserted. Given these results, an *ab initio* study of such systems is, indeed, of interest. Furthermore, C_{60} also adopts an icosahedral structure, and, therefore, the double-shell systems of $C_{60}@Au_{60}^{4+,6-}$ are investigated further using TD-DFT to compare *ab initio* results to those obtained from the classical simulations.

To properly account for possible interactions between the Au_{60} and C_{60} buckyballs, the non-hybrid functional TPSS has been exchanged by its advanced local hybrid relative, the modified PSTS functional (mPSTS). Using Mulliken population analysis, we find that for the anionic species, a significant part of the excess electrons is located on the C_{60} fullerene, summing to 3.5 electrons being located on the fullerene. This is in good agreement with previous findings of the electron acceptor capabilities of C_{60}.[63] Curiously, this is raised to nearly 4.3 excess electrons in the cationic species, which was not anticipated. This hints at the Au_{60} buckyball being rather electron deficient in the cationic species.

The obtained TD-mPSTS spectra for the cationic and anionic cases are shown in Figs. 5 and 6, respectively. First, we observe that the stand-alone Au_{60} spectra of both species (blue lines) have changed significantly with respect to the spectrum shown in Fig. 3. The overall decrease in absorption can be related to two different issues. First, the geometrical re-optimization of Au_{60}, caused by the fullerene, already leads to a decrease in the maximum molar absorption coefficient of roughly 35%, as can be seen from the stand-alone, but re-optimized Au_{60} spectra in Figs. 5 and 6 (blue lines). Second, just like in the classical simulation, inserting the C_{60} fullerene suppresses the optical absorption even further (red lines).

Starting from $C_{60}@Au_{60}^{4+}$ and adding ten electrons, i.e., filling the next shell with h_u symmetry toward the $C_{60}@Au_{60}^{6-}$, lead to only a very slight change in geometry. In addition, the absorption spectra of the (deformed) stand-alone Au_{60} structures are rather similar for both cases. In Figs. 5 and 6, we find three resonances in the optical energy region below 3 eV (blue lines), one around 1.8 eV, another one in the bulk plasmon band around 2.3–2.4 eV, and finally close to 2.8 eV.

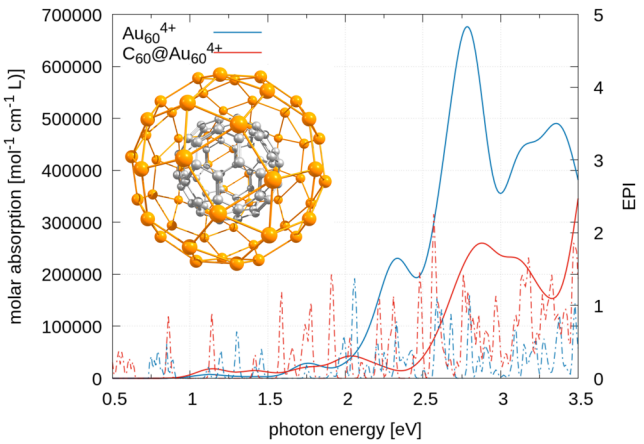

FIG. 5. Comparison of the absorption spectra of $C60@Au_{60}^{4+}$ and Au_{60}^{4+}, obtained from TD-mPSTS/dhf-TZVPP (solid lines). Spectra of Au_{60}^{4+} obtained at the $C_{60}@Au_{60}^{4+}$ geometry. An arbitrary Gaussian broadening of 0.10 eV has been applied. The dashed-dotted lines present the associated EPI values, which have been broadened by 0.01 eV.

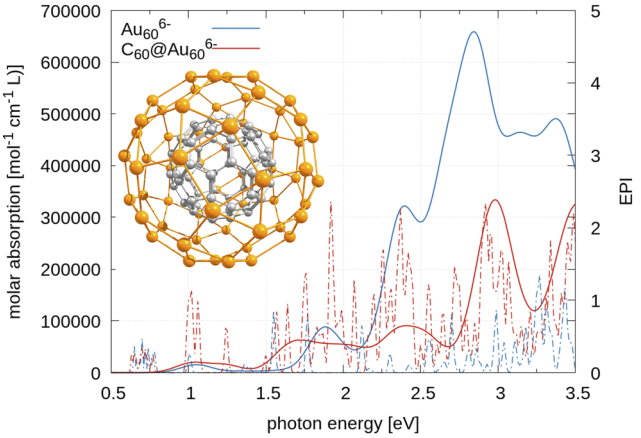

FIG. 6. Comparison of the absorption spectra of C60@Au_{60}^{6-} and Au_{60}^{6-}, obtained from TD-mPSTS/dhf-TZVPP (solid lines). Spectra of Au_{60}^{6-} obtained at the C_{60}@Au_{60}^{6-} geometry. An arbitrary Gaussian broadening of 0.10 eV has been applied. The dashed-dotted lines present the associated EPI values, which have been broadened by 0.01 eV.

The spectra of the combined structures in Figs. 5 and 6 (red lines) exhibit broad absorption shoulders of relatively small intensity that range from 1.5 to 2.5 eV. Moreover, a prominent mode resides around 3 eV both for the cationic and anionic species.

It is remarkable that the drop in intensity is accompanied by a rise in the overall plasmonic character as judged by the EPI. We partly attribute the loss in intensity to the loss in electron density caused by the C_{60} fullerene, as indicated by the Mulliken population analysis. In general, significantly increased EPI values are obtained for the combined double-shell structure. As the EPI is strictly independent of the absolute value of the absorption cross section (or the related molar absorption), this, indeed, indicates that the C_{60}@Au_{60} compounds exhibit a higher plasmonic character than the stand-alone Au_{60} both for the anionic and the cationic species. Especially in the *anionic* species, the band around 2.4 eV in Fig. 6 shows a high density of high-valued EPI excitations. Additionally, the mode at 3 eV turns out to behave equally plasmonic in the sense of the EPI, although it was quite inconspicuous previously in the stand-alone structure and was not accompanied with significant EPI indication. The *cationic* compound surprisingly lacks a relevant molar absorption in the band around the classical bulk plasmon between 2.0 and 2.5 eV in Fig. 5. Moreover, the EPI values are strongly suppressed there, indicating that depleting the shell by removing ten electrons with respect to the anionic case strongly disturbs the plasmon. We hypothesize that the plasmonic excitation has been shifted to higher frequencies as it might be concluded by the emergence of a rather broad double-peak resembling mode between 2.5 and 3.3 eV, where we again notice a high density of high-valued EPI excitations.

IV. CONCLUSION

This study considered single- and double-shell molecular systems to model and investigated quantum plasmonic excitations. The near-spherical Au_{60} particle provides a convenient way to investigate and assess plasmonic excitations at a molecular level. On the one hand, the system is compact enough to be accessible by high-level *ab initio* methods such as TD-DFT based on modern local hybrid functionals. On the other hand, the system is large enough to be well approximable with macroscopic electrodynamics in the T-matrix approach. Our results obtained from both frameworks agree and reproduce the same qualitative behavior. The energy-based plasmonicity index (EPI) was extended to the realm of TD-DFT, providing a way to rapidly evaluate the plasmonic character of an excitation, making them distinguishable from molecular single-particle excitations in quantum systems. Based on Eq. (19), the index can easily be evaluated from the eigenvectors obtained from the TD-DFT eigenvalue problem with a vanishing overhead. Therefore, the EPI can be easily applied even to many (hundreds or thousands) of excited states within seconds to a few minutes of processing time, which is a major improvement for future studies that aim at designing quantum plasmonic devices from scratch.

Further investigations of previously envisioned molecular C_{60}@Au_{60} double-shell compounds composed of Au_{60} and C_{60} buckyballs exhibit that the double-shell system reduces the overall absorption cross section significantly, both in quantum mechanical and classical simulations. However, we find an increased plasmonicity index, hinting at the excitations in such double-shell systems to possess a significant plasmonic character.

SUPPLEMENTARY MATERIAL

See the supplementary material for excited state energies, oscillator strengths, and EPI values for all molecular systems investigated. For generating the graphs, solely the oscillator strength in the length representation, marked as "Osc.(len)," has been used.

ACKNOWLEDGMENTS

M.M.M. acknowledges financial support through the Research Travel Grant by the Karlsruhe House of Young Scientists (KHYS). M.M.M. and C.R. acknowledge support by the Deutsche Forschungsgemeinschaft (DFG, German Research Foundation) (Project No. 378579271) within Project No. RO 3640/8-1. N.P. and C.R. acknowledge support by the Deutsche Forschungsgemeinschaft (DFG, German Research Foundation) (Project No. 413974664) within Project No. RO 3640/12-1. C.H. and C.R. acknowledge financial support from the VolkswagenStiftung.

AUTHOR DECLARATIONS

Conflict of Interest

The authors have no conflicts to disclose.

DATA AVAILABILITY

The data that support the findings of this study are available within the article and its supplementary material.

REFERENCES

[1]M. A. Cazalilla, J. S. Dolado, A. Rubio, and P. M. Echenique, "Plasmonic excitations in noble metals: The case of Ag," Phys. Rev. B **61**, 8033–8042 (2000).
[2]V. Giannini, A. I. Fernández-Domínguez, S. C. Heck, and S. A. Maier, "Plasmonic nanoantennas: Fundamentals and their use in controlling the radiative properties of nanoemitters," Chem. Rev. **111**, 3888–3912 (2011).
[3]F. H. L. Koppens, D. E. Chang, and F. J. García de Abajo, "Graphene plasmonics: A platform for strong light-matter interactions," Nano Lett. **11**, 3370–3377 (2011).
[4]M. S. Tame, K. R. McEnery, Ş. K. Özdemir, J. Lee, S. A. Maier, and M. S. Kim, "Quantum plasmonics," Nat. Phys. **9**, 329–340 (2013).
[5]G. W. Bryant, E. Waks, and J. R. Krenn, "Plasmonics: The rise of quantum effects," Opt. Photonics News **25**, 50–53 (2014).
[6]S. I. Bozhevolnyi and N. A. Mortensen, "Plasmonics for emerging quantum technologies," Nanophotonics **6**, 1185–1188 (2017).
[7]C. Lee, B. Lawrie, R. Pooser, K.-G. Lee, C. Rockstuhl, and M. Tame, "Quantum plasmonic sensors," Chem. Rev. **121**, 4743–4804 (2021).
[8]G. Giannone, S. Śmiga, S. D'Agostino, E. Fabiano, and F. Della Sala, "Plasmon couplings from subsystem time-dependent density functional theory," J. Phys. Chem. A **125**, 7246–7259 (2021).
[9]N. Asadi-Aghbolaghi, R. Rüger, Z. Jamshidi, and L. Visscher, "TD-DFT+TB: An efficient and fast approach for quantum plasmonic excitations," J. Phys. Chem. C **124**, 7946–7955 (2020).
[10]F. Alkan and C. M. Aikens, "TD-DFT and TD-DFTB investigation of the optical properties and electronic structure of silver nanorods and nanorod dimers," J. Phys. Chem. C **122**, 23639–23650 (2018).
[11]M. Kuisma, A. Sakko, T. P. Rossi, A. H. Larsen, J. Enkovaara, L. Lehtovaara, and T. T. Rantala, "Localized surface plasmon resonance in silver nanoparticles: Atomistic first-principles time-dependent density-functional theory calculations," Phys. Rev. B **91**, 115431 (2015).
[12]T. P. Rossi, M. Kuisma, M. J. Puska, R. M. Nieminen, and P. Erhart, "Kohn–Sham decomposition in real-time time-dependent density-functional theory: An efficient tool for analyzing plasmonic excitations," J. Chem. Theory Comput. **13**, 4779–4790 (2017).
[13]J. Yan, K. W. Jacobsen, and K. S. Thygesen, "Conventional and acoustic surface plasmons on noble metal surfaces: A time-dependent density functional theory study," Phys. Rev. B **86**, 241404 (2012).
[14]B.-J. Wang, Y. Xu, and S.-H. Ke, "Plasmon excitations in sodium atomic planes: A time-dependent density functional theory study," J. Chem. Phys. **137**, 054101 (2012).
[15]K. Zhang and H. Zhang, "Plasmon coupling in gold nanotube Assemblies: Insight from a time-dependent density functional theory (TDDFT) calculation," J. Phys. Chem. C **118**, 635–641 (2014).
[16]S.-M. Mullins, H.-C. Weissker, R. Sinha-Roy, J. J. Pelayo, I. L. Garzón, R. L. Whetten, and X. López-Lozano, "Chiral symmetry breaking yields the *I*-Au_{60} perfect golden shell of singular rigidity," Nat. Commun. **9**, 3352 (2018).
[17]O. Lopez-Acevedo, J. Akola, R. L. Whetten, H. Grönbeck, and H. Häkkinen, "Structure and bonding in the ubiquitous icosahedral metallic gold cluster $Au_{144}(SR)_{60}$," J. Phys. Chem. C **113**, 5035–5038 (2009).
[18]H. Qian and R. Jin, "Controlling nanoparticles with atomic precision: The case of $Au_{144}(SCH_2CH_2Ph)_{60}$," Nano Lett. **9**, 4083–4087 (2009).
[19]D. Bahena, N. Bhattarai, U. Santiago, A. Tlahuice, A. Ponce, S. B. H. Bach, B. Yoon, R. L. Whetten, U. Landman, and M. Jose-Yacaman, "STEM electron diffraction and high-resolution images used in the determination of the crystal structure of the $Au_{144}(SR)_{60}$ cluster," J. Phys. Chem. Lett. **4**, 975–981 (2013).
[20]J. M. Jacobo-Fernández and A. Tlahuice-Flores, "Effect of the charge state on the structure of the Au_{60} cluster," Phys. Chem. Chem. Phys. **23**, 442–448 (2021).
[21]S. Bernadotte, F. Evers, and C. R. Jacob, "Plasmons in molecules," J. Phys. Chem. C **117**, 1863–1878 (2013).
[22]E. B. Guidez and C. M. Aikens, "Quantum mechanical origin of the plasmon: From molecular systems to nanoparticles," Nanoscale **6**, 11512–11527 (2014).
[23]A. Lauchner, A. E. Schlather, A. Manjavacas, Y. Cui, M. J. McClain, G. J. Stec, F. J. García de Abajo, P. Nordlander, and N. J. Halas, "Molecular plasmonics," Nano Lett. **15**, 6208–6214 (2015).
[24]J. Gao, W. Zou, W. Liu, Y. Xiao, D. Peng, B. Song, and C. Liu, "Time-dependent four-component relativistic density-functional theory for excitation energies. II. The exchange-correlation kernel," J. Chem. Phys. **123**, 054102 (2005).
[25]F. Wang, T. Ziegler, E. van Lenthe, S. van Gisbergen, and E. J. Baerends, "The calculation of excitation energies based on the relativistic two-component zeroth-order regular approximation and time-dependent density-functional with full use of symmetry," J. Chem. Phys. **122**, 204103 (2005).
[26]M. Kühn and F. Weigend, "Implementation of two-component time-dependent density functional theory in TURBOMOLE," J. Chem. Theory Comput. **9**, 5341–5348 (2013).
[27]C. Holzer, "An improved seminumerical Coulomb and exchange algorithm for properties and excited states in modern density functional theory," J. Chem. Phys. **153**, 184115 (2020).
[28]M. M. Müller, M. Kosik, M. Pelc, G. W. Bryant, A. Ayuela, C. Rockstuhl, and K. Słowik, "Energy-based plasmonicity index to characterize optical resonances in nanostructures," J. Phys. Chem. C **124**, 24331–24343 (2020).
[29]L. Bursi, A. Calzolari, S. Corni, and E. Molinari, "Quantifying the plasmonic character of optical excitations in nanostructures," ACS Photonics **3**, 520–525 (2016).
[30]R. Zhang, L. Bursi, J. D. Cox, Y. Cui, C. M. Krauter, A. Alabastri, A. Manjavacas, A. Calzolari, S. Corni, E. Molinari, E. A. Carter, F. J. García de Abajo, H. Zhang, and P. Nordlander, "How to identify plasmons from the optical response of nanostructures," ACS Nano **11**, 7321–7335 (2017).
[31]M. Guerrini, A. Calzolari, D. Varsano, and S. Corni, "Quantifying the plasmonic character of optical excitations in a molecular J-aggregate," J. Chem. Theory Comput. **15**, 3197–3203 (2019).
[32]G. Mie, "Beiträge zur optik trüber medien, speziell kolloidaler metallösungen," Ann. Phys. **330**, 377–445 (1908).
[33]C. Bohren and D. R. Huffman, in *Absorption and Scattering of Light by Small Particles*, Wiley Science Paperback Series, edited by C. Bohren and D. R. Huffman (Wiley-VCH, 1998).
[34]I. Fernandez-Corbaton, D. Beutel, C. Rockstuhl, A. Pausch, and W. Klopper, "Computation of electromagnetic properties of molecular ensembles," ChemPhysChem **21**, 878–887 (2020).
[35]R. Alaee, C. Rockstuhl, and I. Fernandez-Corbaton, "Exact multipolar decompositions with applications in nanophotonics," Adv. Opt. Mater. **7**, 1800783 (2019).
[36]M. I. Mishchenko, L. D. Travis, and A. A. Lacis, *Scattering, Absorption, and Emission of Light by Small Particles* (Cambridge University Press, Cambridge, 2002).
[37]MATLAB version 9.5.0.944444 (R2018b), The Mathworks, Inc., Natick, MA, 2018.
[38]M. E. Casida, "Time-dependent density functional response theory for molecules," in *Recent Advances in Density Functional Methods* (World Scientific, Singapore, 1995), pp. 155–192.
[39]R. Bauernschmitt and R. Ahlrichs, "Treatment of electronic excitations within the adiabatic approximation of time dependent density functional theory," Chem. Phys. Lett. **256**, 454–464 (1996).
[40]R. E. Stratmann, G. E. Scuseria, and M. J. Frisch, "An efficient implementation of time-dependent density-functional theory for the calculation of excitation energies of large molecules," J. Chem. Phys. **109**, 8218–8224 (1998).
[41]F. Furche and R. Ahlrichs, "Adiabatic time-dependent density functional methods for excited state properties," J. Chem. Phys. **117**, 7433–7447 (2002).
[42]M. Liu, T.-W. Lee, S. K. Gray, P. Guyot-Sionnest, and M. Pelton, "Excitation of dark plasmons in metal nanoparticles by a localized emitter," Phys. Rev. Lett. **102**, 107401 (2009).
[43]S.-C. Yang, H. Kobori, C.-L. He, M.-H. Lin, H.-Y. Chen, C. Li, M. Kanehara, T. Teranishi, and S. Gwo, "Plasmon hybridization in individual gold nanocrystal dimers: Direct observation of bright and dark modes," Nano Lett. **10**, 632–637 (2010).
[44]D. Solis, B. Willingham, S. L. Nauert, L. S. Slaughter, J. Olson, P. Swanglap, A. Paul, W.-S. Chang, and S. Link, "Electromagnetic energy transport in nanoparticle chains via dark plasmon modes," Nano Lett. **12**, 1349–1353 (2012).
[45]D. E. Gómez, Z. Q. Teo, M. Altissimo, T. J. Davis, S. Earl, and A. Roberts, "The dark side of plasmonics," Nano Lett. **13**, 3722–3728 (2013).

[46]E. Townsend and G. W. Bryant, "Plasmonic properties of metallic nanoparticles: The effects of size quantization," Nano Lett. **12**, 429–434 (2012).
[47]E. Townsend and G. W. Bryant, "Which resonances in small metallic nanoparticles are plasmonic?," J. Opt. **16**, 114022 (2014).
[48]E. Townsend, A. Debrecht, and G. W. Bryant, "Approaching the quantum limit for nanoplasmonics," J. Mater. Res. **30**, 2389–2399 (2015).
[49]L. Bursi, A. Calzolari, S. Corni, and E. Molinari, "Light-induced field enhancement in nanoscale systems from first-principles: The case of polyacenes," ACS Photonics **1**, 1049–1058 (2014).
[50]M. M. Müller, M. Kosik, M. Pelc, G. W. Bryant, A. Ayuela, C. Rockstuhl, and K. Słowik, "Modification of the optical properties of molecular chains upon coupling to adatoms," Phys. Rev. B **104**, 235414 (2021).
[51]M. M. Müller, M. Kosik, M. Pelc, G. W. Bryant, A. Ayuela, C. Rockstuhl, and K. Słowik, "From single-particle-like to interaction-mediated plasmonic resonances in graphene nanoantennas," J. Appl. Phys. **129**, 093103 (2021).
[52]C. M. Aikens, S. Li, and G. C. Schatz, "From discrete electronic states to plasmons: TDDFT optical absorption properties of Ag_n (n = 10, 20, 35, 56, 84, 120) tetrahedral clusters," J. Phys. Chem. C **112**, 11272–11279 (2008).
[53]L. J. Zhao, L. Jensen, and G. C. Schatz, "Pyridine–Ag_{20} cluster: A model system for studying surface-enhanced Raman scattering," J. Am. Chem. Soc. **128**, 2911–2919 (2006).
[54]J. Yan, Z. Yuan, and S. Gao, "End and central plasmon resonances in linear atomic chains," Phys. Rev. Lett. **98**, 216602 (2007).
[55]J. Tao, J. P. Perdew, V. N. Staroverov, and G. E. Scuseria, "Climbing the density functional ladder: Nonempirical meta-generalized gradient approximation designed for molecules and solids," Phys. Rev. Lett. **91**, 146401 (2003).
[56]F. Weigend and A. Baldes, "Segmented contracted basis sets for one- and two-component Dirac–Fock effective core potentials," J. Chem. Phys. **133**, 174102 (2010).
[57]E. Caldeweyher, S. Ehlert, A. Hansen, H. Neugebauer, S. Spicher, C. Bannwarth, and S. Grimme, "A generally applicable atomic-charge dependent London dispersion correction," J. Chem. Phys. **150**, 154122 (2019).
[58]J. P. Perdew, V. N. Staroverov, J. Tao, and G. E. Scuseria, "Density functional with full exact exchange, balanced nonlocality of correlation, and constraint satisfaction," Phys. Rev. A **78**, 052513 (2008).
[59]C. Holzer, Y. J. Franzke, and M. Kehry, "Assessing the accuracy of local hybrid density functional approximations for molecular response properties," J. Chem. Theory Comput. **17**, 2928–2947 (2021).
[60]S. G. Balasubramani, G. P. Chen, S. Coriani, M. Diedenhofen, M. S. Frank, Y. J. Franzke, F. Furche, R. Grotjahn, M. E. Harding, C. Hättig, A. Hellweg, B. Helmich-Paris, C. Holzer, U. Huniar, M. Kaupp, A. Marefat Khah, S. Karbalaei Khani, T. Müller, F. Mack, B. D. Nguyen, S. M. Parker, E. Perlt, D. Rappoport, K. Reiter, S. Roy, M. Rückert, G. Schmitz, M. Sierka, E. Tapavicza, D. P. Tew, C. van Wüllen, V. K. Voora, F. Weigend, A. Wodyński, and J. M. Yu, "TURBOMOLE: Modular program suite for *ab initio* quantum-chemical and condensed-matter simulations," J. Chem. Phys. **152**, 184107 (2020).
[61]J. C. Slater, "Atomic radii in crystals," J. Chem. Phys. **41**, 3199–3204 (1964).
[62]B. Song, H. Gu, S. Zhu, H. Jiang, X. Chen, C. Zhang, and S. Liu, "Broadband optical properties of graphene and HOPG investigated by spectroscopic Mueller matrix ellipsometry," Appl. Surf. Sci. **439**, 1079–1087 (2018).
[63]E. Brocl/awik and A. Eilmes, "Density functional study of endohedral complexes M@C_{60} (M = Li, Na, K, Be, Mg, Ca, La, B, Al): Electronic properties, ionization potentials, and electron affinities," J. Chem. Phys. **108**, 3498–3503 (1998).
[64]M. Kehry, Y. J. Franzke, C. Holzer, and W. Klopper, "Quasirelativistic two-component core excitations and polarisabilities from a damped-response formulation of the Bethe–Salpeter equation," Mol. Phys. **118**, e1755064 (2020).